Open access • Journal Article • DOI:10.1021/ACS.JPCC.0C03083

# A Multitechnique Study of Fluorinated Nanodiamonds for Low-Energy Neutron Physics Applications — Source link

Michael Herraiz, Nicolas Batisse, Marc Dubois, Valery Nesvizhevsky ...+4 more authors

**Institutions:** European Synchrotron Radiation Facility, University of La Laguna

**Published on:** 02 Jul 2020 - Journal of Physical Chemistry C (ACS Publications)

**Topics:** Neutron, Scattering and Amorphous carbon

# A Multi Technique Study of Fluorinated Nanodiamonds for Low-Energy Neutron Physics Applications

*M. Herraiz,[‡] N. Batisse,[‡] M. Dubois,[‡,*] V.V. Nesvizhevsky,[†] C. Cavallari,[+] M. Brunelli,[•] V. Pischedda,[#] S. Radescu [□]*

‡ Université Clermont Auvergne, Sigma Clermont (ICCF), 24, avenue Blaise Pascal 63178 Aubière, France.

† Institut Max von Laue – Paul Langevin, 71 avenue des Martyrs, 38042 Grenoble cedex, France.

+ ESRF- The European Synchrotron Radiation Facility, 38042 Grenoble cedex, France.

• Dutch-Belgian Beamline DUBBLE at the ESRF, Grenoble cedex, France.

# Institut Lumière Matière, UMR5306 Université Lyon 1-CNRS, Université de Lyon 69622 Villeurbanne cedex, France.

□ Departamento de Física, Instituto de Materiales y Nanotecnología, MALTA Consolider Team, Universidad de La Laguna, La Laguna, E-38205 Tenerife, Spain

**ABSTRACT**

Data of quasi-specular reflection of cold neutrons, prompt-γ neutron analysis, X-ray Raman scattering (XRS) and neutron Pair distribution function (PDF) analysis with powder of detonation nanodiamonds are analyzed to collect their structural properties and chemical composition. Both as-synthesized and purified were studied using fluorination samples. Removal of both $sp^2$ amorphous carbon shell and hydrogen atoms is evidenced respectively by the change of neutron-nuclei optical potentials of nanoparticles and the increase of their neutron reflectivity. Moreover, $sp^3$ diamond cores of nanoparticles stay intact during the fluorination as revealed by similar scattering patterns, PDF and XRS data. Quasi-specular reflection, PDF and XRS data are complementary for the study of nanomaterials and in good agreement with conventional characterization techniques (infrared spectroscopy and solid-state NMR).

## 1. INTRODUCTION

Fine investigation of nanomaterials needs a combination of complementary characterization techniques in order to collect information at different scales concerning their structure and chemical composition. The perfect knowledge of those characteristics allows a rational use of the nanomaterials. In the present paper, we apply non-conventional techniques to characterize nanodiamonds (*NDs*) powders[1,2], after purification under molecular fluorine flux[3,4]. As a matter of fact, nanodiamond powder combines high volume density of diamond, high coherent scattering length ($b^C$ = 6.65 fm), low neutron absorption ($\sigma_{abs}{}^C$ = 3.5 mb) and inelastic scattering cross-sections of C. *NDs* can be efficiently used in low-energy neutron physics due to the quasi-

specular reflection of cold neutrons (CNs) at small incidence angle to powder surface[5,6,7,8] and the diffusive reflection of very cold neutrons (VCNs) at any incidence angle[9,10,11,12].

Cross-sections of neutron scattering on *NDs* have been studied in detail[13,14]. These investigations compare, in particular, different techniques of producing NDs and measure temperature dependence of inelastic scattering cross-sections. The authors show virtual absence of low-energy excitations thus highly elastic neutron scattering and underline the importance of clustering or agglomeration of nanoparticles in powders for neutron diffusion and transport. Important efforts have been devoted for including the diffusion of slow neutrons in the DND powder to neutron transport simulations[15,16].

X-ray Raman Scattering (XRS) and Pair Distribution Function analysis (PDF) are both bulk techniques very sensitive to the atomic local structure and C hybridization. PDF is a well-established technique for studying disordered or semi-ordered materials while XRS is a non-resonant inelastic X-ray scattering technique that allows observing the core electron excitation in the sample and thus the unoccupied electronic density of states[17,18]. XRS uses X-rays in the hard regime, giving a penetration depth in the order from hundreds of micrometers to millimeters. Prompt-γ neutron analysis allows the absolute evaluation of hydrogen content[19]. Neutrons scattering represents a powerful method[20,21,22,23] to study the size, shape and positions of scatter. Quasi-specular reflection of CNs may be used for the general purpose of characterization of nanomaterials in addition to conventional techniques such as XRD, Raman and solid-state NMR.

*NDs* can be produced in the nanocrystalline form, by the detonation of carbon-containing explosives such as trinitrotoluene and hexogen in a steel chamber[1,24]. Pressure increase during the explosion allows a high diamond content to be obtained in the detonation soot. Using this method, metal impurities and carbon phases distinct from diamond, such as amorphous carbons,

graphite, and fullerene-like carbons, can be synthesized in addition to nanodiamonds, and the resulting samples are then usually described as a diamond core ($sp^3$ carbons) which is covered by a $sp^2$ carbon fullerene-like shell. The shell structure and its thickness depend on the detonation condition. Because a unique combination of properties that nanodiamonds provide, such as nanometric size (variable according to the synthesis route), low cost, chemical inertness of diamond core whereas their surface may be easily functionalized, negligible toxicity, excellent mechanical (exceptional hardness, fracture strength) and optical properties and scalable production, they are potentially used in numerous applications in biology, and medicine[25,26,27]. In particular, *NDs* are promising materials for building slow neutron reflectors. Their size allows miniaturized mechanical systems and devices (MEMS), cantilevers and gears. For most of these fields, a suitable surface termination and functionalization of the diamond materials are required and a pure surface is needed. Detonation *NDs* are chemically treated with $F_2$ gas for purification purpose. For future applications, a very precise characterization of the final product is essential. In order to probe the local structure in the core of the *NDs*, we have employed XRS and PDF of neutron diffraction. PDF provides straightforward information about the local structure in terms of first neighboring distances. XRS allows the direct observation of soft X-rays edges (like C and F K edges) of bulk samples thanks to the use of hard X-rays that are inelastically scattered[17,18]. Both techniques are therefore sensitive to the C-hybridization and local structure with a bulk penetration depth. Data from quasi-specular reflection of cold neutrons, PDF and XRS will be compared to conventional techniques such as XRD, solid state NMR, Raman and infrared spectroscopies in order to clarify in great details the structure of *NDs* and evidence the efficiency of the new techniques. *Ab initio* theoretical calculations for bulk diamond and the diamond (111)

H-terminated surface were performed within the framework of the density functional theory (DFT).

## 2 METHODS

**2.1 Materials.** *NDs* were fluorinated in static conditions using a two-step process in a closed Nickel reactor. *NDs* were placed onto passivated Nickel supports (covered with $NiF_2$) inside the reaction vessel. Prior to the fluorine gas insertion, the reactor was evacuated to primary vacuum ($\sim 10^{-2}$ mbar) for 12 hours. A flux of pure fluorine gas (99.9% purity) was then added to reach 0.6 atm inside the reactor. This condition was fixed in order to avoid pressure higher than 1.2 atm during heating and decomposition gas evolution resulting from the fluorination. The temperature was increased to 450 °C and then stabilized for 12 h. After this first treatment and cooling to room temperature, the reactor was flushed with nitrogen flow for 1 hour to remove unused fluorine, HF and decomposition products ($CF_4$, $C_2F_6$, …)[28]. For the completion of both $sp^2$ layer and hydrogen removal, the same vacuum/fluorine insertion/fluorination at 450 °C for 12h/evacuation/cooling sequence was carried out in the second step. On the one hand, with such a two-step treatment, amorphous carbons located onto the *ND* surface must totally decompose into gaseous $CF_4$ and $C_2F_6$; weight loss of the sample was then expected. On the other hand, formation of covalent C-F bonds resulted in weight uptake. Finally, the weight change is very low during the treatment, less than 2 wt%, also highlighting the stability of the *NDs* under these drastic conditions. The resulting samples are then denoted *F-NDs*.

**2.2 Neutron Diffraction Data for PDF Analysis.** Neutron diffraction data (more details can be found in[29]) were collected at the neutron diffractometer for disordered materials D4C at

the ILL (Institut Laue Langevin, Grenoble, FR)[30]. We used an incident wavelength λ= 0.4989 Å corresponding to a maximum Q of 23.5 $Å^{-1}$. Powder samples were placed inside a sealed 7 mm diameter Vanadium cylindrical cell and measured at room temperature in a vacuum. In order to obtain the PDF function, prior to the space-Fourier transform, an appropriated background and multiple corrections were applied to the raw data using the *CORRECT* program[31]. All the data reduction and treatment were done using the routines available on the instruments[32].

**2.3 X-ray Raman Scattering.** X-ray Raman scattering (XRS) data were collected on the dedicated XRS spectrometer of the beamline ID20 of the European Synchrotron ESRF (Grenoble, France)[33]. The beam was monochromatized, using a nitrogen cooled Si (111) monochromator and a Si (311) Channel Cut post-monochromator and focussed at the beam position by two mirrors in Kirkpatrick-Baez geometry. Beam size was approximately 10 × 20 $μm^2$ (V × H). 36 spherically bent Si(660) analyzer crystals at the final energy $E_f$ of 9.8 KeV and 3 area Maxipix detectors[34] were used on collected inelastically scattered photons from the sample. The overall energy resolution was 0.7 eV and the mean momentum transfer was 3.2 ± 0.3 $Å^{-1}$. The powder samples were placed into *ad-hoc* grooved flat Aluminium sample holder and their position could be adjusted thanks to the goniometer stage of a Huber tower. The incident beam angle was 10 degrees. All data were collected at room temperature. Raw data from pixelated images were treated using the XRS tools python routines, as described elsewhere[35].

**2.4 Quasi-Specular Reflection, Neutron Prompt-$\gamma$ Analysis and Conventional Methods.** Quasi-specular reflection of cold neutrons was measured at D17 neutron reflectometer[36] at ILL. Experimental details are given in reference[7].

In order to measure very small residual amounts of H after the powder purification, we applied the neutron prompt-$\gamma$ analysis method as in [37] but used a much more intense neutron

beam (PF1B instrument at the ILL[38]). To minimize the background in this measurement, we, on one hand, placed powder samples in thin-walls aluminum envelopes with a low hydrogen content, and, on the other hand, carefully protected the germanium γ-detector against scattered neutrons and γ-quanta. The count-rate in the $\gamma$-quanta peak of total absorption of the reaction $n(p,d)\gamma$ ($E_\gamma = 2.223\ Mev$) allowed measuring $H$ content in the sample and in the empty envelope used as background. The absolute calibration of the $\gamma$-quanta detection efficiency in the H peak was carried out using a thin polyethylene sample with a precisely known amount of $H$.

FTIR spectrometer NICOLET 5700 (Thermo Electron) was used to record IR spectra using both ATR and transmission modes. 100 scans with 4 $cm^{-1}$ resolution were collected to acquire each spectrum between 4000 and 400 $cm^{-1}$. The single-reflection ATR accessory (Thermo Scientific Smart Orbit) is working with a durable diamond crystal (type IIa Diamond tungsten carbide mounted in stainless steel with a refractive index of 2.4 and an incident angle of 58°) and a swivel pressure tower that ensured consistent pressure from sample to sample. The active sample area was 1.5 $mm^2$. A wide spectral range (10000 to below 200 $cm^{-1}$) and good depth of penetration (DP of 2.03 μm at 1000 $cm^{-1}$) were then reached. NMR experiments were carried out on a Bruker Avance spectrometer with operating frequency of 282.2 $^{19}F$. A simple sequence ($\tau$-acquisition) was used with a single $\pi/2$ pulse length of 5.5 μs and the recycle time was equal to 5 s. $^{19}F$ chemical shifts were referenced to $CFCl_3$.

**2.4 Ab initio Theoretical Calculations with Density Functional Theory (DFT).** The structural optimizations were performed within the DFT framework using the VASP code[39] (in a PAW-PBE scheme[40]) with similar settings as in previously published papers[41,42]. The integrations over the Brillouin zone (BZ) were carried out using the Monkhorst-Pack scheme with a 15x15x1 grid for the calculation on the slab. The slab was modelled as a hydrogen

terminated diamond surface, with five bilayers of carbon atoms in hexagonal (111) planes. The vacuum region between the periodically repeated images of the slab was approximately 14 Å. We have also carried out calculations of the core level binding energies for the C-1s core state, including final-state core hole effects (core-level relaxation energy), which involve the recalculation of the Kohn-Sham eigenvalues for the core states for the chosen atom using a half core-hole[43]. The C-1s energy values is referred to the electrostatic potential at vacuum. For the calculation of the vibrational properties (and the subsequent assignment of the modes based upon the symmetry analysis of the eigenvector) we used the density functional perturbation theory (DFPT) and the PHONOPY software package[44].

## 3. RESULTS AND DISCUSSION

Prompt-$\gamma$ analysis showed that $H$ content in *NDs* is drastically reduced by the fluorination, achieving the level of 4 $ppm$, which is 35-60 times lower than that before fluorination. The H/C atomic ratio are equal to $7.5 \pm 0.2$ and $430 \pm 30$ for *NDs* and *F-NDs* respectively. Quantitative NMR using polytetrafluoroethylene (PTFE) as an internal reference (Fig. 1) gives a chemical composition $CF_{0.097}$. Two types of C-F bonds are highlighted: on diamond core ($CF_{0.079\pm0.005}$) and due to the fluorination of the residual $sp^2$ carbon shell ($CF_{0.018\pm0.005}$). As a matter of fact, according to their nature, C-F bonds exhibit $^{19}F$ chemical of -164 ppm or -190 ppm. For fluorine linked to $sp^3$ carbon, the chemical shift depends on its neighboring: when C–F bonds are present, $\delta_{19F}$ is equal to -190 ppm whereas if the neighboring consists in non-fluorinated $sp^3$ carbons the chemical shift is of -164 ppm (case of $(C_2F)_n$ type graphite fluoride). This is related to the interaction between fluorine and the neighboring, which weakens the C–F covalence. The lower the C–F covalence, the higher the chemical shift[45,46]. The line at -164 ppm is the main

component for *F-NDs*. The shoulders at -184 and -200 ppm indicates the presence in very low amounts of C-F bonds, which are due to the fluorination of $sp^2$ carbon atoms (denoted $C_{ex\text{-}sp2}F$ in Fig. 1); all the $sp^2$ carbons are not decomposed into gaseous species ($CF_4$ and $C_2F_6$). The multi-nuclear NMR data are further discussed in supplementary information, Fig. SI2).

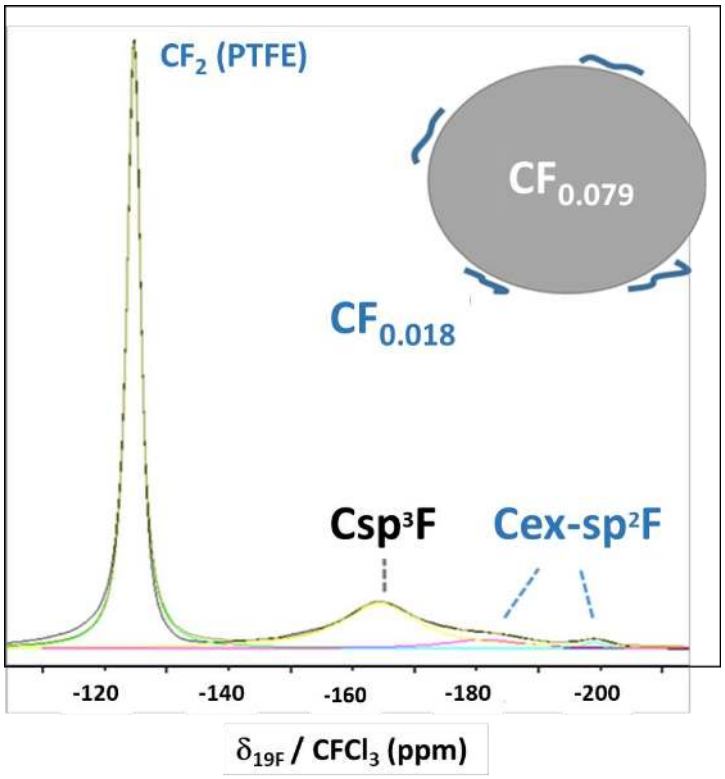


Fig. 1. $^{19}F$ MAS NMR (30 kHz) of fluorinated NDs mixed with PTFE reference for quantification purpose.

**3.1 Structural Characterization.** Neutron PDF data reveals the maintaining of a diamond core after fluorination (Fig. 2) in good accordance with X-ray diffraction[3]. The patterns essentially coincide for raw and fluorinated NDs, indicating a well-preserved prevalence of C-C distances of the diamond structure. Interatomic distances don't show any appreciable variations after fluorinations. The first distances appear at 1.54, 2.52 and 2.95 Å as expected for first C-C neighbors in $Csp^3$ diamond structure. No appreciable difference in the PDF patterns of *NDs* and

*F-NDs* can be noticed. The technique, giving the bulk-average distances, does not appear to be sensitive to the little amount of F in *F-NDs*. The calculated DFT distances on bulk $sp^3$-diamond are in excellent agreement with the distances calculated by PDF method i.e. 1.546, 2.526 and 2.962 Å. X-ray small angle scattering was stronger for the fluorinated sample, when scaled to the intensity of the diffraction lines[3]; it was interpreted as the reduction of size of whole particles (diamond core plus shell) related to the destruction of graphite shell and/or disappearance of absorption layer. The average size of diamond core was evaluated via the Scherrer formula from the broadening at half the maximum intensity (after subtracting the instrumental line broadening contribution) of the diffraction lines. The result of 4.3 nm has to be taken with caution, as derived for monodispersed population[3].

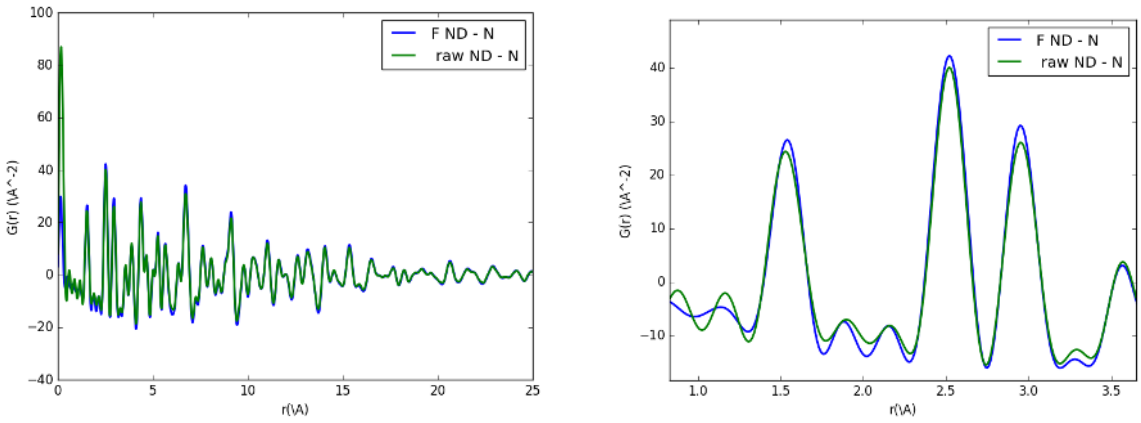


Fig. 2. Experimental neutron PDFs of raw and fluorinated *NDs* plotted up to r =25 Å (left panel) and magnifications, collected at the diffractometer D4C (ILL, Grenoble), using an incident neutron wavelength λ= 0.4989 Å and Q max = 23.5 $Å^{-1}$.

**3.2 X-ray Raman Scattering and Spectroscopic Characterization.** XRS was used to investigate the electronic and local atomic structure of *NDs*, before and after the fluorination process. XRS spectra at the C K-edge and F K-edge are presented in Figure 3.

The XRS spectra of graphite and diamond powders are reported from reference [29] as an example of pure $Csp^2$ and $Csp^3$ hybridization[47]. As discussed in refs [29] and [47], the main features of the C absorption edge are associated to the transitions of the C 1s electron of the empty π and σ states in the conduction band. These states are indicated in Figure 3 as π* (in graphite only) and σ*.

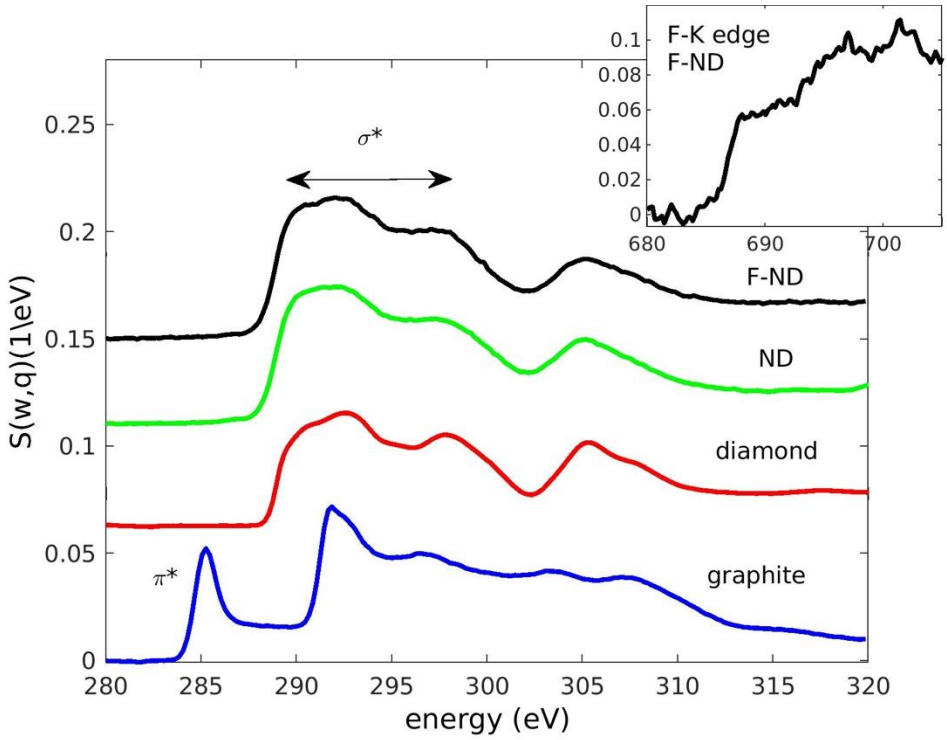


Fig. 3. XRS spectra at the Carbon K edge of *F-NDs*, NDs, graphite and diamond powder. Graphite and diamond powders are reported as an example of pure $Csp^2$ and $Csp^3$ hybridization (data published in [29]). In the inset, XRS spectra at the F-K edge for *F-NDs*.

Data of *NDs* and *F-NDs* clearly confirm the preservation of C - $sp^3$ hybridization as in diamond powder. From the computational results, we obtain a value of 285.6 eV for the C1s core level binding energy.

Indeed, datasets for the two nanodiamond samples appear very similar to the one of diamond powder, in agreement with diffraction data[3]. This indicates the preservation of a predominant diamond-like core, also after fluorination. The excitonic feature at the σ* band threshold as well as the band itself are globally less defined than in diamond powder; this is more evident in *F-NDs*, probably indicating a small loss of crystallinity due to the fluorination process. XRS spectra of the two nano-powders looks globally very similar, except for the presence of a tiny inelastic feature at around 690 eV in *F-NDs*. This corresponds to the F-K edge transition. Because of the very little amount of F in *F-NDs*, the feature appears very noisy and ill-defined; even if it is possible to notice a main edge located at 687 eV, in very good agreement for what observed from C-F covalent bonds in the $C_1F$ and $C_2F$ fluorinated graphites[Erreur ! Signet non défini.29].

To summarize, XRS highlights three mains features i) no traces of $sp^2$ shell are detected for *NDs* and *F-NDs* ii) $sp^3$ core is unaffected by the fluorination (in accordance with PDF data), and iii) residual amount of covalent C-F bonds is detected for *F-NDs*. Those results are in good accordance with conventional FTIR and solid state NMR spectroscopies (Figs. SI2a and b)[3]. Raman spectroscopy is highly sensitive to carbonaceous materials either with $sp^2$ or $sp^3$ hybridization; tt allowed discriminating the carbon hybridization state[3]. As a matter of fact, the Raman spectrum of a single-crystal bulk diamond exhibits a $T_{2g}$ symmetry band at 1332 $cm^{-1}$ with a full width at half maximum (fwhm) in the 2.2/4.6 $cm^{-1}$ range[48,49,50]. The vibrational study on bulk diamond shows a peak at 1296.4 $cm^{-1}$ ($T_{2g}$ symmetry), and for the diamond surface at 1299.6 $cm^{-1}$ (C-C bond). Amorphous carbons typically exhibit G band close to 1600 $cm^{-1}$ and the disorder-induced double-resonance D band in the 1250–1400 $cm^{-1}$ [51,52]. Moreover, presence of O–H and carbonyl groups on $sp^2$- or $sp^3$-hybridizated carbon atoms (pseudo-G band) results in an additional band at 1624 $cm^{-1}$ [53,54]. In addition to the narrow band of diamond carbons at 1332

$cm^{-1}$, the bands at 1325 and 1624 $cm^{-1}$ were observed for the raw *NDs* spectrum[3], highlighting the presence of both residual $sp^2$ carbon atoms of the fullerene-like (or onion-like) shell as well as O–H and/or carbonyl containing functional groups. Those additional bands disappeared after the fluorination showing the removal of both the $sp^2$ layer and oxygen containing groups. FTIR spectra give additional information about the total removal of OH groups (Fig. 4); the assignment of the vibration modes is reported on the figure. The broad bands in the 3280–3675 $cm^{-1}$ (Fig. 4b) range and at 1640 $cm^{-1}$ (Fig. 4a), which are related respectively to O–H stretching and bending vibrations[53,55,56] disappear after the fluorination in agreement with Raman data. It is to note that the band at 1640 $cm^{-1}$ may be assigned to C=C vibration. Carbon atoms involved in such bonds are also removed as seen by highly sensitive Raman spectroscopy. C-H bonds can be also underlined by the presence of the band at 2900 $cm^{-1}$. Vibrational DFT calculations yield a peak at 2928.4 $cm^{-1}$ for the H-terminated (111) diamond surface which is related to the $C_{sp3}$-H bond.

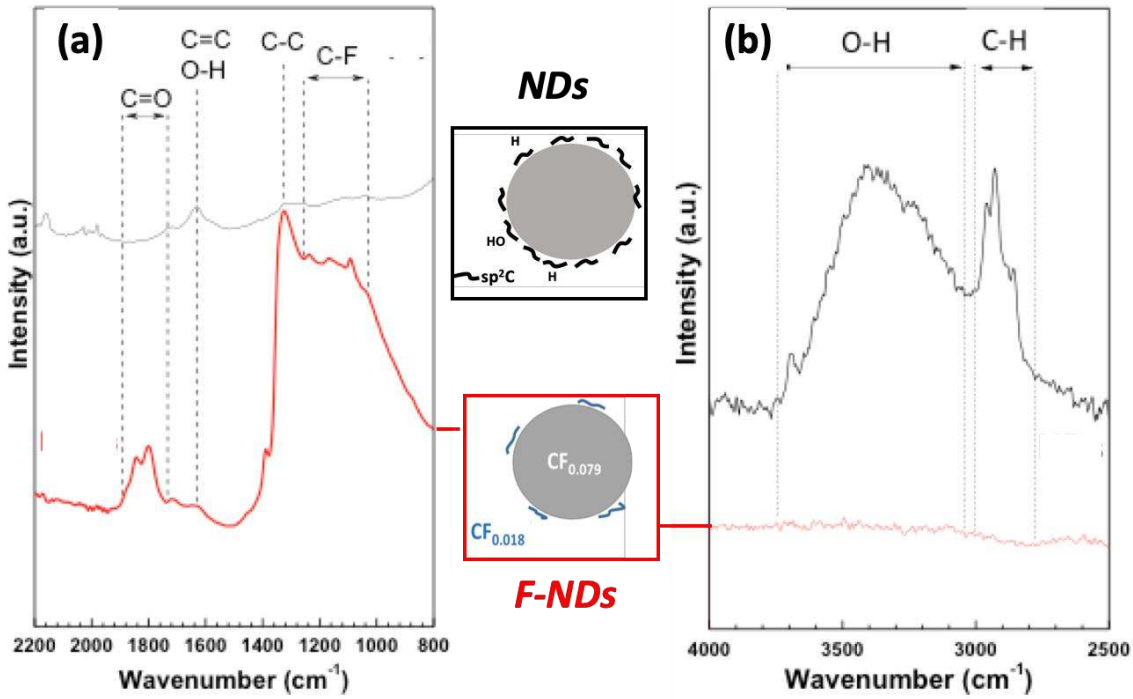


Fig. 4. FTIR spectra (ATR mode) of raw and fluorinated *NDs*.

Because C-H is converted into C-F during the treatment, the line is not present after the treatment. Surprisingly, the intensity of C=O band increases after fluorination. An IR spectrum of the raw sample is ill-defined due to the conductive carbonaceous shell on the diamond core and the C=O vibration band may be hindered. Nevertheless, FTIR and Raman spectroscopies evidence qualitatively the removal of C-OH and C-H groups as well as the $sp^2$ carbons layer onto the diamond core.

**3.3 Quasi-Specular Reflection.** Here, we analyze the method of neutron quasi-specular reflection from the point of view of information about the studied samples that it can provide. Fig. 5 shows an example of scattering data measured with *NDs* and *F-NDs*. Reference 7 indicates the experiment geometry.

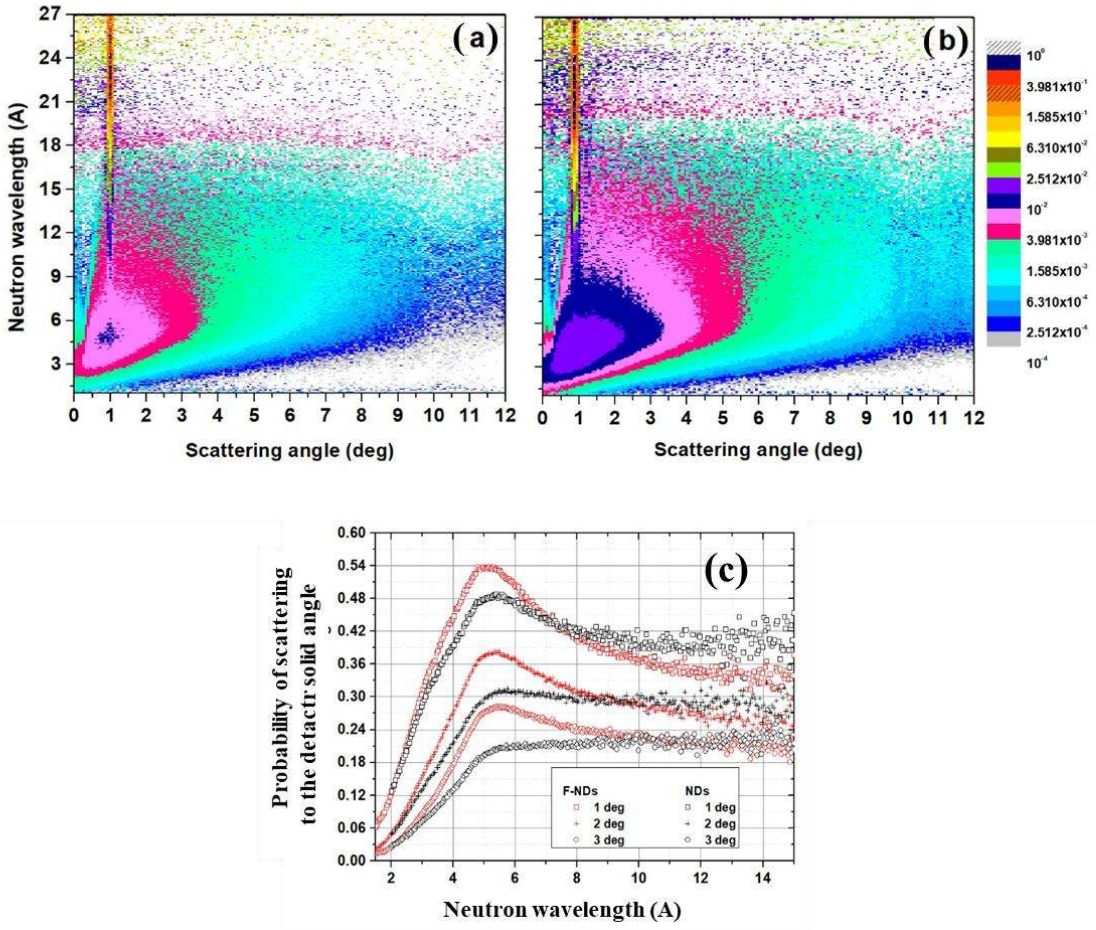


Fig. 5. An example of quasi-specular scattering data measured with *NDs* (Fig. 5a) and *F-NDs* (Fig. 5b) samples at D17 instrument at ILL. Different intensities/colors (in the insert on right) indicate a relative number of neutrons, as a function of scattering angle (X-axis, in degrees) and neutron wavelength (Y-axis, in Å). The neutron incidence angle equals $1^{o}$. Fig. 5c. Differential probability of neutron scattering, measured as a function of neutron wavelength (Å), from *F-NDs* (in red) and *NDs* (in black) to the angular acceptance of D17 detector in the geometry indicated in Fig. SI1. We integrated data over the whole range of scattering angles, and normalized them to total incident intensity. The incidence angle is $1^{o}$, $2^{o}$, and $3^{o}$, respectively, as indicated in the insert.

The main factor determining the patterns of quasi-specular reflection is neutron scattering on diamond cores of nanoparticles. Therefore, the general similarity of the patterns measured with the two studies samples (Fig. 5a and Fig. 5b) means that the fluorination effect on $sp^3$ cores is small or absent, in agreement with XRS.

Nevertheless, some excess in the probability of quasi-specular reflection from a fluorinated powder (Fig. 5b) over the probability of reflection from a raw powder (Fig. 5a) indicates a change in its properties. This change becomes better visible after integration the scattering patterns over the whole range of scattering angles Fig. 5c; the results for *F-NDs* and *NDs* were compared for the incidence angle of $1^o$, $2^o$ and $3^o$, respectively. Presentation of experimental data in the format of Fig. 5c is also useful for analyzing the effect of neutron diffraction in diamond cores of nanoparticles.

Diffraction diffuses neutrons to large angles thus eliminating them from quasi-specular directions. The cut-off wavelength for diamond is twice the (111) interplanar distance, or 4.12 Å. The cut-off is not sharp due to broadening associated with finite nanoparticle sizes; as a result, the diffraction suppression extends towards ~5Å. The scale of this broadening is inversely proportional to the size of the nanoparticles. Using this simple consideration, it is straightforward to estimate a mean size of diamond $sp^3$ cores. However, an accurate calculation of the mean size, as well as the size distribution of diamond cores, will require the development of a theory that takes into account neutron diffraction by small size diamond nuclei of arbitrary shape, as well as the exact contribution of this effect to the probability of quasi-specular reflection of neutrons.

Fig. 5c also shows that the mean difference between the scattering curves is a significantly larger probability of quasi-specular reflection of neutrons from fluorinated nanoparticle powder at the neutron wavelengths of 4-5 Å. This difference is due to the scattering

of neutrons to large angles in reflection from the raw powder, in particular in the $sp^2$ C shells with respectively larger interatomic distances than those in the diamond. Thus, we conclude about the removal of nanoparticle shells consisting of $sp^2$ carbon due to fluorination.

The overall efficiency of quasi-specular reflection is improved with *F-NDs*. Such effect is due to fluorination, which had removed $sp^2$ shell from the nanoparticles and hydrogen contaminations[17]. This purification occurs without major changes in the diamond core.

## 4. CONCLUSION

A set of complementary non-conventional techniques were applied to characterize nanodiamond powders. In particular, the effect of purification using fluorination was investigated. Fluorination process appears effective in drastically reducing the H content and $sp^2$ carbon layer at the surface of *NDs*, thought preserving the $sp^3$ diamond core. PDF and XRS highlight the maintaining of the diamond core during fluorination without structural change. Quasi-specular reflection of CNs from powder of raw *NDs* and purified *NDs* indicates the removal of $sp^2$ C layer. Prompt-γ neutron analysis evidences the drastically reduced H content. On one hand, purified *NDs* are confirmed to be much more efficient neutron reflectors for CNs and VCNs. On the other hand, we have shown that XRS and neutron quasi-specular reflection are powerful characterization techniques. The methods can be applied to powders of any nanoparticles (not only nanodiamonds) provided the particle size ranges from a few to a few tens of nanometers.

## AUTHOR INFORMATION

### Corresponding Author

*Marc Dubois, Marc.dubois@uca.fr, 0033473407105

ACKNOWLEDGMENT

These measurements and sample characterization were performed at the ID20 and ID23 beamlines at ESRF, in Grenoble (France).

Neutron measurements were performed at D4C, PF1B, D17 and D11 instruments at ILL, in Grenoble (France). [doi:10.5291/ILL-DATA.6-06-479],[doi:10.5291/ILL-DATA.3-07-386], [doi:10.5291/ILL-DATA.TEST-2772], [doi:10.5291/ILL-DATA.3-07-361]. The authors are grateful to all instrument responsibles, as well as to our GRANIT and SLON collaborators, for their help during measurements and useful discussions.

S.R. acknowledges the support from MINECO Project No. MAT2016-75586-C4-3-P. This work was supported by the LABEX iMUST (ANR-10-LABX-0064) of Université de Lyon, within the program *"Investissements d'Avenir"* (ANR-11-IDEX-0007) operated by the French National Research Agency (ANR).

This work is supported by grant ERC INFRASUP P-2019-1/871072, CREMLINplus Grant agreement 871072 and RFFI-18-29-19039 grant.

**REFERENCES**


[1] de Carli, P. J.; Jameieson, J. C. Formation of diamond by explosive shock. *Science* **1961**, 133, 1821-1822.

[2] Aleksenskii, A. E.; Baidakova, M. V.; Vul', A. Y.; Siklitskii, V. I. The structure of diamond nanoclusters. *Phys. Solid State* **1999**, 41, 668-671.

[3] Nesvizhevsky, V. V.; Koester, U.; Dubois, M.; Batisse, N.; Frezet, L.; Bosak, A.; Gines, L.; Williams, O. Fluorinated nanodiamonds as unique neutron reflector, *Carbon* **2018**,1 30, 799-805.

[4] Nesvizhevsky, V. V.; Koester, U.; Dubois, M.; Batisse, N.; Frezet, L.; Bosak, A.; Gines, L.; Williams, O. Fluorinated nanodiamonds as unique neutron reflector. *J. Neutron Res.* **2018**, 20, 81-82.

[5] Remizovich, V. S. Theoretical description of elastic reflection of particles (photons) incident at grazing angles without the use of the diffusion approximation. *JETP* **1984**, 60, 290-299.

[6] Nesvizhevsky, V.; Cubitt, R.; Lychagin, E.; Muzychka, A.; Nekhaev, G.; Pignol, G.; Protasov, K.; Strelkov, A. Application of diamond nanoparticles in low-energy neutron physics. *Materials* **2010**, 3, 1768-1781.

[7] Cubitt, R.; Lychagin, E. V.; Muzychka, A. Y.; Nekhaev, G. V.; Nesvizhevsky, V. V.; Pignol, G.; Protasov, K. V.; Strelkov, A. V. Quasi-specular reflection of cold neutrons from nano-dispersed media at above-critical angles. *Nucl. Instr. Meth. A* **2010**, 622, 182-185.

[8] Nesvizhevsky, V. V.; Dubois, M.; Gutfreund, Ph.; Lychagin, E. V.; Yu. Nezvanov A.; Zhernenkov, K. N. Effect of nanodiamond fluorination on the efficiency of quasispecular reflection of cold neutrons. *Phys. Rev. A* **2018**, 97, 023629.

[9] Nesvizhevsky, V.V. Interaction of neutrons with nanoparticles. *Phys. At. Nucl.* **2002**, 65, 400-408.

[10] Lychagin, E. V.; Muzychka, A. Y.; Nesvizhevsky, V. V.; Pignol, G.; Protasov, K. V.; Strelkov, A. V. Storage of very cold neutrons in a trap with nanostructured walls. *Phys. Lett. B* **2009**, 679, 186-190.

[11] Nesvizhevsky, V. V.; Lychagin, E. V.; Muzychka, A.Y .; Strelkov, A. V.; Pignol, G.; Protasov, K. V. The reflection of very cold neutrons from diamond powder nanoparticles. *Nucl. Instr. Meth. A.* **2008**, 595, 631-636.

[12] Artem'ev, V. A. Estimation of neutron reflection from nanodispersed materials. *At. En.* **2006**, 101, 901-904.

[13] Ersez, T.; Osborn, J. C.; Lu, W.; Mata, J. P. Small angle and inelastic scattering investigation of nanodiamonds. *Physica B* **2018**, 551, 278-282.

[14] Teshigawara, M.; Tsuchikawa, Y.; Ichikawa, G.; Takata, S.; Mishima, K.; Harada, M.; Ooi, M.; Kawamura, Y.; Kai, T.; Ohira-Kawamura, S. et al. Nuclear Instruments and Methods in Physics Research Section A: Accelerators, Spectrometers, Detectors and Associated Equipment. *Nucl. Instrum. Meth.* **2019**, A 929, 113-120.

[15] Jamalipour, M.; Zanini, L.; Gorini, G. Directional reflection of cold neutrons using nanodiamond particles for compact neutron sources. *EPJ Web Conf.* **2020**, 231, 04003.

[16] Granada, J. R.; Damain, J. I.; Helman, Ch. Studies on Reflector Materials for Cold Neutrons. *EPJ Web Conf.* **2020**, 231, 04002.

[17] Suzuki, T. X-ray Raman scattering experiment. *J. Phys. Soc. Jpn* **1967**, 22, 1139-1150.

[18] Huotari, S.; Pylkkänen, T.; Soininen, J. A.; Kas, J. J.; Hämäläinen, K.; Monaco, G. X-ray Raman scattering based EXAFS beyond the dipole limit. *J. Synchrotron Radiat.* **2012**, 19, 106-113.

[19] Lindstrom, R.; Paul, R. L.; Vincent, D.; Greenberg, R. Measuring hydrogen by cold-neutron prompt-gamma activation analysis. *J. Radioanal. Nuc. Ch.* **1994**,180(2), 271-275.

[20] Schelten, J.; Shmatz, W. Multiple-scattering treatment for small-angle scattering problems. *J. Appl. Crystallogr.* **1980**, Vol. 13, 385-390.

[21] Maleev, S. V.; Toperverg, B. P. Low-angle multiple scattering by static inhomogeneities. *JETP Lett.* **1980**, Vol. 78, 315-330.

[22] Feigin, L. A.; Svergun, D. I. in: Structure Analysis by Small-Angle X-Ray and Neutron Scattering. *Plenum Press*, **1987**.

[23] Sabine, T. M.; Bertram, W. K. The use of multiple-scattering data to enhance small-angle neutron scattering experiments. *Acta Crystallogr. A.* **1999**, 55, 500-507.

[24] Gruen, D. M. Nanocrystalline diamond films. *Annu. ReV. Mater. Sci.* **1999**, 29, 211–259.

[25] Krueger, A.; Lang, D.; Functionality is Key: Recent Progress in the Surface Modification of Nanodiamond. *Adv. Funct. Mater.* **2012**, 22, 890–906.

[26] Vadym Mochalin, N.; Shenderova, O.; Ho, D.; Gogotsi, Y. The properties and applications of nanodiamonds, *Nature Nanotechnology* **2012**, 7, 11–23.

[27] Turcheniuk, K.; Mochalin V. N. Biomedical applications of nanodiamond. *Nanotechnology* **2017**, 23, 8(25), 252001.

[28] Peyroux, J.; Dubois, M.; Tomasella, E.; Petit, E., Flahaut, D. Enhancement of surface properties on commercial polymer packaging films using various surface treatment processes (fluorination and plasma). *Appl. Surf. Sci*. **2014**, 315, 426-431.

[29] Cavallari, C.; Brunelli, M.; Radescu, S.; Dubois, M.; Batisse, N.; Vaughan, G. B. M.; Fischer H. E.; Pischedda V. Structural and electronic changes in graphite fluorides as a function of fluorination rate: an XRS, PDF and DFT study. *Carbon* **2019**, 147,1-8 .

[30] Fischer, H.; Cuello, G.; Palleau, P.; Feltin, D.; Barnes, A.; Badyal, Y.; Simonson, J. D4c: A very high precision diffractometer for disordered materials. *Applied Physics A* **2002**, 74 (1) s160 - s162.

[31] Howe, M. A.; McGreevy R. L.; Zetterström P. *CORRECT: A correction program for neutron diffraction data*. NFL, Uppsala University, **1996**.

[32] Fischer, H. E.; Barnes, A. C.; Salmon. P. S.; Neutron and x-ray diffraction studies of liquids and glasses. *Rep. Progr. Phys.* **2006**, 69, 233–299.

[33] Huotari, S.; Sahle, C. J.; Henriquet C.; Al-Zein, A.; Martel, K.; Simonelli, L.; Verbeni, R.; Gonzalez, H.; Lagier, M.-C.; Ponchut, C. et al. A large-solid-angle X-ray Raman scattering spectrometer at ID20 of the European Synchrotron Radiation Facility. *J. Synchrotron Rad.* **2017,** 24(2), 521–530.

[34] Ponchut C.; Rigal, J. M.; Clément, J.; Papillon, E.; Homs A.; Petitdemange, S. MAXIPIX, a fast readout photon-counting X-ray area detector for synchrotron applications. *J. Inst*. **2011**, 6, C01069.

[35] Sahle, C. J.; Mirone A.; Niskanen, J.; Inkinen, J.; Krisch, M.; Huotari S. Planning, performing and analyzing X-ray Raman scattering experiments. *J. Synchrotron Rad.* **2015**, 22, 400-409.

[36] Cubitt, R.; Fragneto, G. D17: the new reflectometer at the ILL . *Appl. Phys. A* **2002**, 74, S329.

[37] Krylov, A. R.; Lychagin, E. V.; Muzychka, A. Y.; Nesvizhevsky, V. V.; Nekhaev, G. V.; Strelkov, A. V.; Ivanov, A. S. Study of bound hydrogen in powders of diamond nanoparticles. *Crystal. Rep.* **2011**, 7, 1186-1196.

[38] Abele, H.; Dubbers, D.; Hase, H.; Klein, M.; Knopfer, A.; Kreuz, M.; Lauer, T.; Markisch, B.; Mund, D.; Nesvizhevsky et al. Characterization of a ballistic supermirror neutron guide. *Nucl. Instr. Meth. A* **2006**, 562, 407-417.

[39] Kresse G.; Furthmüller J. Efficient iterative schemes for ab initio total-energy calculations using a plane-wave basis set. *Phys. Rev. B* **1996**; 54(16), 11169-11186.

[40] Perdew, J. P.; Ruzsinszky, A.; Csonka, G. I.; Vydrov, O. A.; Scuseria, G. E.; Constantin, L. A.; Zhou, X.; Burke K. Restoring the Density-Gradient Expansion for Exchange in Solids and Surfaces. *Phys. Rev. Lett*. **2008**, 100, 136406.

[41] Pischedda, V.; Radescu, S.; Dubois, M.; Batisse, N.; Balima, F.; Cavallari, C.; Cardenas L. Experimental and DFT high pressure study of fluorinated graphite (C2F)n. *Carbon* **2017**, 114, 690–699.

[42] Pischedda, V.; Radescu, S.; Dubois, M.; Cavallari, C.; Batisse, N.; Balima. F. Fluorine-graphite intercalation compound (C4F)n at high pressure: Experimental and theoretical study. *Carbon* **2018**, 127, 384–391.

[43] Köhler, L.; Kresse. G. Density functional study of CO on Rh(111). *Phys. Rev. B* **2004**, 70 165405.

[44] Togo, A.; Tanaka I. First principles phonon calculations in materials science. *Scr. Mater.,* **2015***,* 108, 1-5.

[45] M. Panich, Nuclear magnetic resonance study of fluorine-graphite intercalation compounds and graphite fluorides. *Synth. Met*. **1999**, vol. 100, 169–185.

[46] M. Dubois, J. Giraudet, K. Guerin, A. Hamwi, Z. Fawal, P. Pirotte, F. Masin, EPR and Solid-State NMR Studies of Poly(dicarbon monofluoride) (C2F)n. *J. Phys. Chem. B* **2006**, vol. 110, 11800–11808.

[47] Ahmad, Y.; Dubois, M.; Guerin, K.; Hamwi, A.; Fawal, Z.; Kharitonov, A. P.; Generalov, A. V.; Yu Klyushin, A.; Simonov, K. A.; Vinogradov, N.A.et al A.S. NMR and NEXAFS Study of Various Graphite Fluorides. *J. Phys. Chem. C* **2013**, 117, 13564–13572.

[48] Yushin, G.N.; Osswald, S.; Padalko, V. I.; Bogatyreva, G. P.; Gogotsi, Y. Effect of sintering on structure of nanodiamond. *Diamond Relat. Mater.* **2005**, 14, 1721–1729.

[49] Prawer, S.; Nugent, K. W.; Jamieson, D. N.; Orwa, J.O.; Bursill, L. A.; Peng, J. L. The Raman spectrum of nanocrystalline diamond. *Chem. Phys. Lett.* **2000**, 332, 93–97.

[50] Yanchuk, I. B.; Ya. Valakh M., Ya. Vul' A., Golubev, V. G.; Grudinkin, S. A.; Feoktistov, N. A. Raman scattering, AFM and nanoindentation characterisation of diamond films obtained by hot filament CVD. *Diamond Relat. Mater*. **2004**, 13, 266–269.

[51] Ferrari, A. C.; Robertson, J. Raman spectroscopy of amorphous, nanostructured, diamond −like carbon, and nanodiamond. *Philos. Trans. R. Soc. London, Ser. A* **2004**, 362, 2477-2452.

[52] Reich, S.; Thomsen, C. Raman spectroscopy of graphite. *Philos. Trans. R. Soc. London, Ser. A* **2004**, 362, 2271–2288.

[53] Osswald, S.; Yushin, G.; Mochalin, V.; Kucheyev, S. O.; Gogotsi, Y. Control of sp2/sp3 carbon ratio and surface chemistry of nanodiamond powders by selective oxidation in air. *J. Am. Chem. Soc.* **2006,** 128, 11635–11642.

[54] Mochalin, V.; Osswald, S.; Gogotsi, Y. Contribution of Functional Groups to the Raman Spectrum of Nanodiamond Powders. *Chem. Mater.* **2009**, 21(2), 273–279.

[55] Spitsyn, B. V.; Denisov, S. A.; Skorik, N. A.; Chopurova, A. G.; Parkaeva, S. A.; Belyakova, L. D.; Larionov, O. G. The physical-chemical study of detonation nanodiamond application in adsorption and chromatography. *Diamond Relat. Mater.* **2010**, 19, 123–127.

[56] Mitev, D.; Dimitrova, R.; Spassova, M.; Minchev, C.; Stavrev, S. Surface peculiarities of detonation nanodiamonds in dependence of fabrication and purification methods. *Diamond Relat. Mater.* **2007**, 16, 776–780.

**TOC GRAPHIC**